Ocean Engineering 290 (2023) 116324

Contents lists available at ScienceDirect

Ocean Engineering

journal homepage: www.elsevier.com/locate/oceaneng

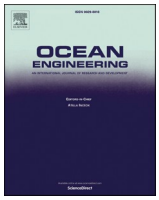

Numerical analysis of the performance of a composite marine propeller blade subject to structural blade oscillations

Shine Win Naung [a,*], Mahdi Erfanian Nakhchi [b], Mohammad Rahmati [b]

[a] School of Engineering, The University of the West of England, Bristol, BS16 1QY, UK
[b] Department of Mechanical and Construction Engineering, Northumbria University, Newcastle upon Tyne, NE1 8ST, UK

ARTICLE INFO

Handling Editor: Prof. A.I. Incecik

Keywords:
Marine propellers
Hydrodynamics
Hydroelasticity
Computational fluid dynamics
Large eddy simulations
Nonlinear frequency domain solution method

ABSTRACT

High-fidelity Large Eddy Simulations (LES) are conducted over the oscillating marine propeller blades to investigate the effects of blade oscillation on the unsteady flow behaviour as well as to analyse the performance of the composite marine propeller blades. The accuracy of the results is first verified against the reference experimental results. A nonlinear frequency-domain solution or harmonic solution method is also applied to this study, based on a high-fidelity LES model, in addition to the traditional time-domain solution method to investigate the capabilities of the frequency-domain method in predicting the unsteady flow parameters, vortex generation, and hydrodynamic damping to determine the stability of the propeller blades. Results obtained reveal that the oscillation of the blade has a great impact on the vortex generation process which could impose implications on the performance and structural integrity of the composite marine propeller blades.

1. Introduction

Ships confront wavy ocean conditions which produce oscillations in the propeller relative to the water. These oscillations cause the propeller to work in off-design conditions. These environment-induced oscillations can significantly affect the propeller performance. Therefore, the performance prediction of marine propellers under turbulent and complex flow conditions requires accurate prediction of the wake and unsteady hydrodynamic parameters of the propeller. Another critical challenge in the design of propeller blades is the flexibility and stiffness of the blades. Using Fibre-Reinforced Polymer (FRP) composite materials can relatively improve the performance of these propellers by maximising the overall propulsive efficiency or minimising the cavitation effects (Vardhan et al., 2019; Gonabadi et al., 2022; Borg et al., 2021). However, the interaction between the propeller blade and the unsteady flow can result in the blade structural oscillation, which, consequently, causes complex flow behaviours and vorticities. Therefore, it is important to resolve the turbulent and transitional flow structures in detail for an accurate prediction of the hydrodynamic performance of the propellers.

Traditionally, marine propellers were made of metals. As mentioned earlier, composite materials, which offer much better strength-to-weight ratios, have been used recently for marine propellers (Pemberton et al., 2018). Moreover, these composite materials provide better structural flexibility and performance subject to unsteady flow conditions. The interaction between the unsteady flow and the elastic structure of the propeller blades can improve the performance of marine ships and reduce the corrosion effects under a wide range of operational conditions (Rama Krishna et al., 2022). Young et al. (2016) investigated the advantages and challenges of adaptive composite materials in marine propulsors. They discussed that the effects of flow-induced vibrations on the performance of the marine rotors should be further investigated. Moreover, smart composite materials such as piezoelectric stiffeners can be used instead of metals to utilise an active control method for the performance improvement of marine propellers (Chen et al., 2017). The main challenge in the modelling of fluid flows over marine propellers made of FRP composite is that typical low-fidelity numerical models cannot sufficiently predict the instantaneous vortex generation and wake profile of the propeller. Due to the elastic behaviour of the blade under different flow conditions, it is deemed necessary to capture the complex phenomena occurred during the fluid-structure interaction process, and therefore, a high-fidelity Computational Fluid Dynamics (CFD) method should be considered (Kumar and Mahesh, 2017).

Several experimental and numerical studies have been conducted to investigate the effects of marine propeller structures on the vortex generation and flow disturbance in the wake region of the blades. Yilmaz

* Corresponding author.
E-mail address: Shine.WinNaung@uwe.ac.uk (S. Win Naung).

https://doi.org/10.1016/j.oceaneng.2023.116324
Received 15 June 2023; Received in revised form 29 October 2023; Accepted 11 November 2023

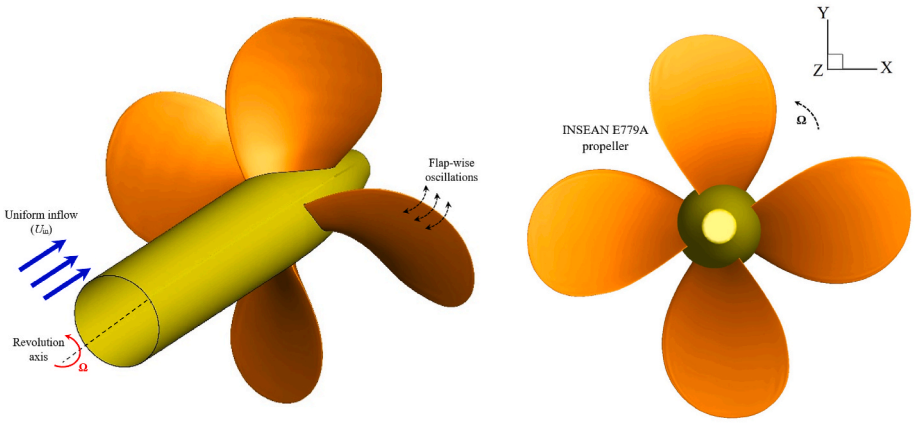

Fig. 1. Geometry of the INSEAN E779A propeller.

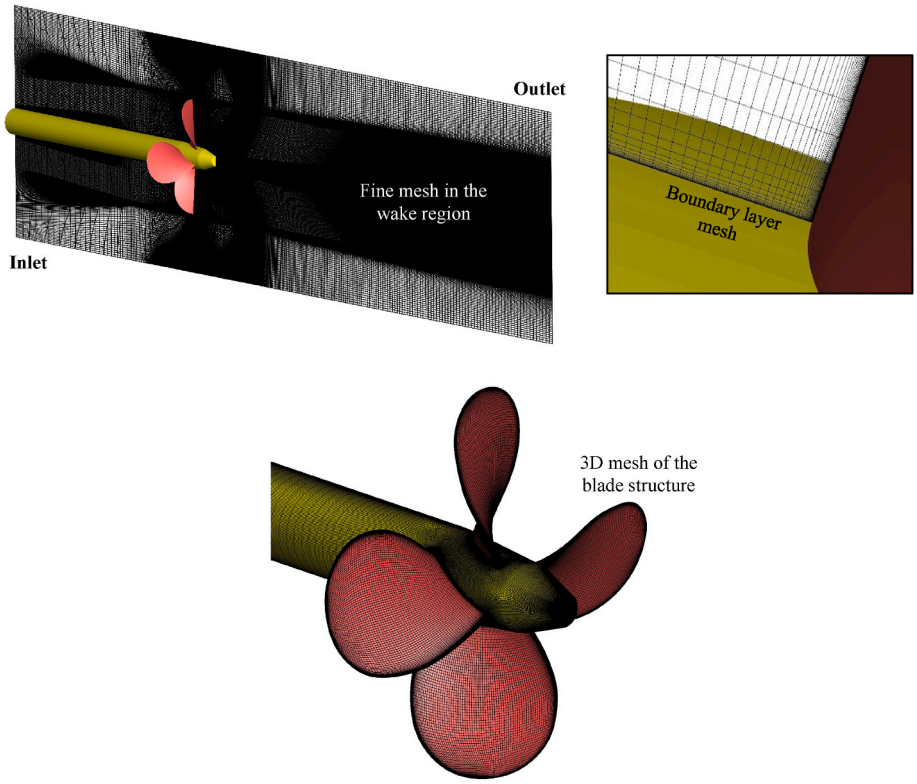

Fig. 2. Representative coarse mesh of the FRP propeller blades.

et al. (2020) investigated, both experimentally and numerically, the phenomena of different types of tip vortex cavitation of a research vessel propeller. Posa et al. (2020) used a Large Eddy Simulation (LES) method to investigate the flow characteristics in the wake region of a propeller. The simulations showed that the spanwise flows within the boundary layer on the blade are linked to the behaviour of the coherent structures generated in the downstream region. Felli et al. (2009) performed an experiment and flow visualisation on the INSEAN E779A propeller, based on the Laser Doppler Velocimetry (LDV) phase-sampling method, to investigate the interaction between the tip vortices and the rudder. Wang et al. (2020) numerically and experimentally investigated the effects of the free surface on the 7-bladed E1658 propeller behind a submarine. They observed that low-fidelity numerical models cannot adequately predict the wake behaviour and the tip vortex generation. In the numerical study of Long et al. (2019), the unsteady cavitating flow around a marine propeller behind the hull was analysed by the k-ω SST turbulence model. It is found that the leading-edge vortex and the side-entrant jet considerably affect the relative vorticity distribution over the propeller blades. Dubbioso et al. (2013) used the Reynolds Averaged Navier-Stokes (RANS) method to investigate the performance of the CNR-INSEAN E779A propeller operating in the oblique flows. They performed simulations for moderate and medium-high propeller loads at $J = 0.60$ and $J = 0.88$, in which $J = U_\infty/nD$ is the advance coefficient of the propeller. They observed that the pressure coefficient distribution is noticeably affected by the blade loads. Muscari et al. (2017) numerically analysed the flow field around a rudder in the wake of the INSEAN E779A marine propeller with the Detached Eddy Simulation (DES) method. The effects of the evolution of tip vorticity due to the interaction with the propeller blade are considered in this study. Moreover, Rahmati (RAHMATI, 2009) developed a pressure correction method, which iteratively updates the continuity equation using a pressure correction technique, to investigate the unsteady flow around

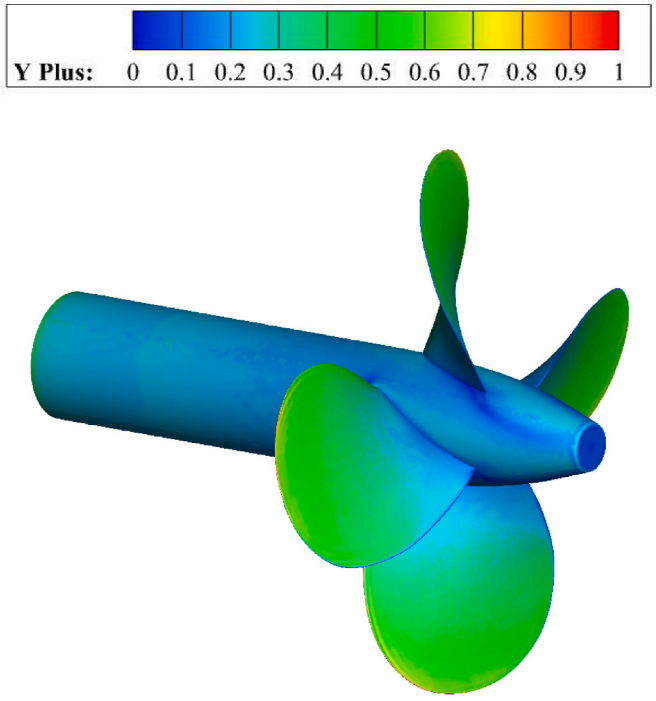

Fig. 3. Y^+ distribution over the propeller hub and blades.

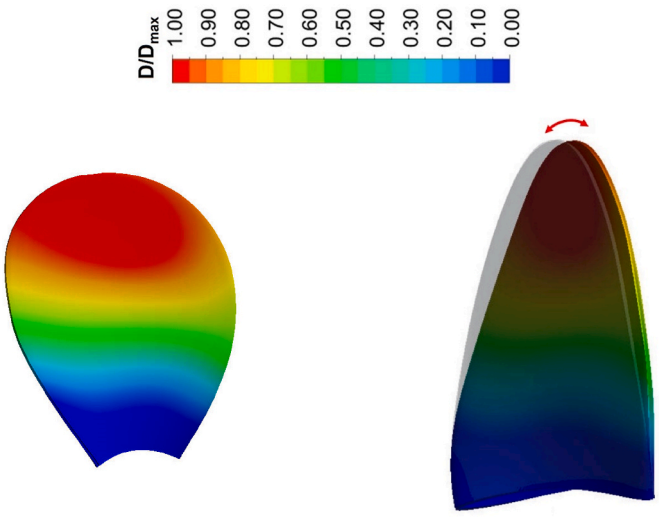

Fig. 4. First vibration mode of the INSEAN E779A propeller.

the E779a propeller.

There are only a few studies in the literature which consider the effects of oscillating propellers. Wang et al. (2018) used the RANS method to numerically investigate the performance of an oscillating propeller in cavity flows. The effects of harmonic vibrations on the four-bladed E779A propeller loads and wake structures were investigated. Politis (2004) performed three-dimensional simulations over an oscillating propeller with a harmonic oscillation function of $y = \frac{D}{4}\sin\left(\frac{\omega t}{2}\right)$. The vortex wake–blade interactions were considered in their simulations. It was observed that their proposed model can capture the wake and pressure distribution under both steady and transient flow conditions. Wang et al. (2017) performed numerical simulations to analyse the performance of an oscillating marine propeller in the cavitating flow. They used the RANS method for their simulations. It was found that the oscillations have an impact on the propeller loads during each oscillatory period. Gong et al. (2018) used the DES method to investigate the wake vortex generation for ducted and non-ducted propellers. Their energy spectrum analysis of the vortex generated in the wake region revealed the growth of wake vortical structures in the temporal domain.

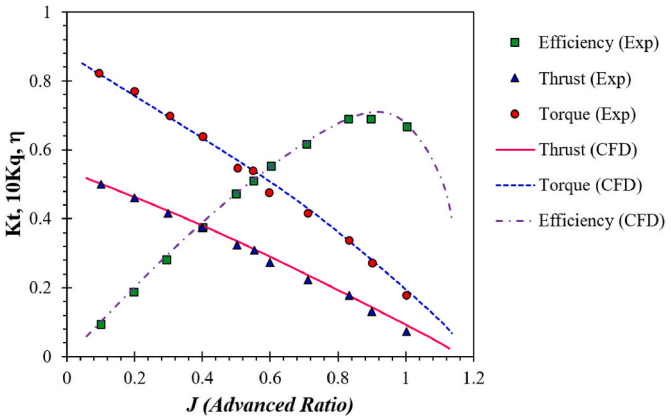

Fig. 5. Performance coefficients of the E779A propeller obtained from the experiment and the present simulations.

The above studies showed that the oscillation of the propeller blades has an impact on the structural load distribution and fatigue could occur in the long term due to the excessive loads on the rotating propellers (Naung et al., 2021a, 2021b). The instantaneous variations of the pressure distributions and loads on the oscillating propeller blades should be monitored. Some experimental studies were conducted on real-time monitoring of loads and strain tensors on composite propeller blades and hydrofoils (Wildy et al., 2010; Phillips et al., 2017). Therefore, it becomes necessary to perform a high-fidelity numerical simulation to capture the instant variations of the propeller blade loads and their impact on additional vorticities due to the fluid-structure interactions between the oscillating propeller blades and water flows.

Based on the above literature review, previous numerical studies on marine propellers were mostly focused on low to mid-fidelity numerical models. In addition, there are no high-fidelity studies on marine propellers made of FRP composite materials using flexible blades. Thus, high-fidelity numerical simulations are performed on composite propellers in this work to capture the details of instantaneous and time-averaged physical parameters on the surface of the propeller blades. Moreover, a high-fidelity CFD model should precisely predict the velocity profile and flow characteristics in the wake region of the composite blade of both rigid and flexible propellers at different amplitudes. In this study, an LES method has been used for the first time to investigate the fluid-structure interaction over a composite propeller blade by considering the flexibility and deformation of the blades using a modal coupling method. A nonlinear frequency-domain solution method, also known as nonlinear harmonic solution method, is applied in addition to the traditional time-domain LES method to investigate the capability of the frequency-domain LES method. The hydrodynamic characteristics over the flexible blades are compared with that of the typical rigid blades to investigate the effects of realistic and complex oscillations of the blades on the unsteady and turbulent flow behaviours.

2. Physical description

The propeller used in this study is a fixed pitch, four-bladed E779A propeller (Pereira et al., 2004) as presented in Fig. 1. The propeller has a diameter (D) of 0.227 m, a pitch ratio (P/D) of 1.1, an expanded area ratio of 0.689, and a hub height ratio of 0.2. Some experimental analyses were performed over this propeller in the INSEAN ship model by Felli et al., 2006, 2011. Fig. 1 depicts the coordinate system used in the numerical simulations, and the propeller rotates around the Z-direction.

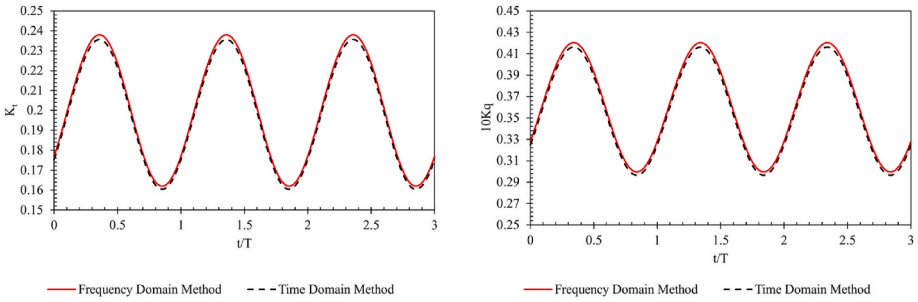

a) Thrust coefficient b) Torque coefficient

Fig. 6. Thrust and torque coefficients of an oscillating propeller (A = 1 mm) obtained from the time-domain method and the frequency-domain method.

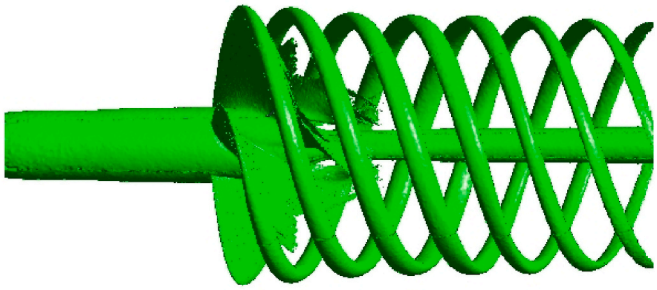

a) Present CFD simulation

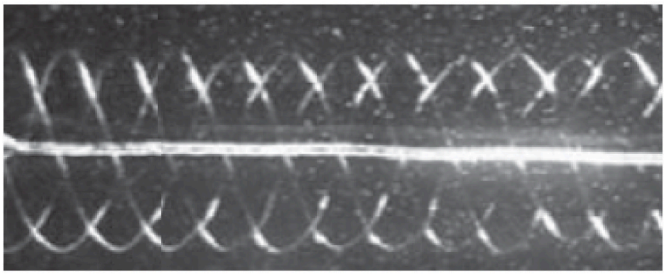

b) Experiment (Felli et al., 2011)

Fig. 7. Propeller wake structures captured by the present CFD simulation and the experiment (Felli et al., 2011).

The direction of uniform inflow velocity (U_{in}) and flap-wise oscillations of the FRP composite blades are also provided.

The mesh generation for the computational domain used for the LES simulation of the propeller blades with the flap-wise blade oscillation is provided in Fig. 2. A three-dimensional structured mesh generator is employed to create a structured mesh, based on a multi-block O4H topology, for the simulations of the INSEAN E779A propeller. A structured multi-block grid is preferred for this analysis due to its capability of providing high-resolution and accurate flow data. The computational domain is decomposed into five blocks, namely the inlet block, outlet block, blade skin block, upper block (located above the blade skin block) and lower block (located below the blade skin block). An O-mesh is employed in the blade skin block and an H-mesh is used in the other blocks. A very small first cell layer thickness is selected to make sure that the y^+ value is kept below unity to fully resolve the laminar viscous sublayer effects (see Fig. 3). The boundary layer mesh is created using a growth rate of 1.2. A fine mesh is employed near the blade tip to precisely capture the tip vorticity and wake fluctuations. In addition, the mesh in both the upstream and downstream regions of the propeller blades is significantly refined to resolve the vorticity and wake structures at different advanced ratios and vibration amplitudes. The generated mesh consists of 14 M cells in a single blade passage, which is found sufficient to perform an LES simulation in this case.

3. Mathematical formulation

The flow around the marine propeller is governed by the Navier-Stokes equations, and a three-dimensional, density-based, finite volume solver is used to solve the unsteady Navier-Stokes equations. The Navier-Stokes equations in the Cartesian frame are given by:

$$\frac{\partial}{\partial t}\int_{\Omega} U d\Omega + \int_{S} \vec{F}.d\vec{S} - \int_{S} \vec{G}.d\vec{S} = \int_{\Omega} S_T d\Omega \quad (1)$$

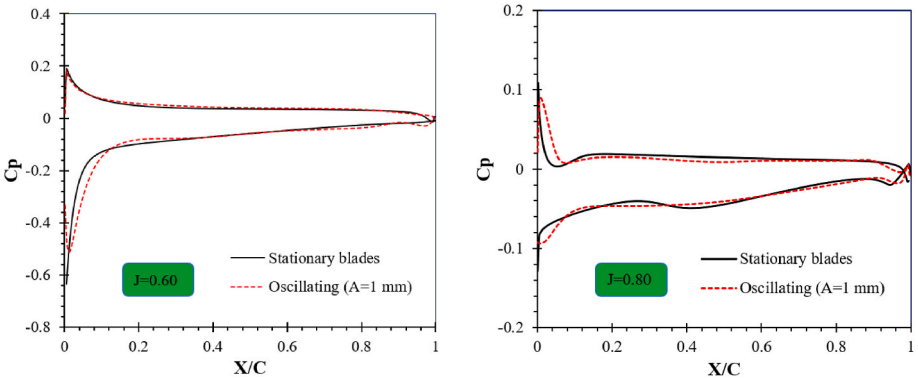

Fig. 8. Pressure coefficient distribution over the oscillating and non-oscillating propeller blades at different advanced rations.

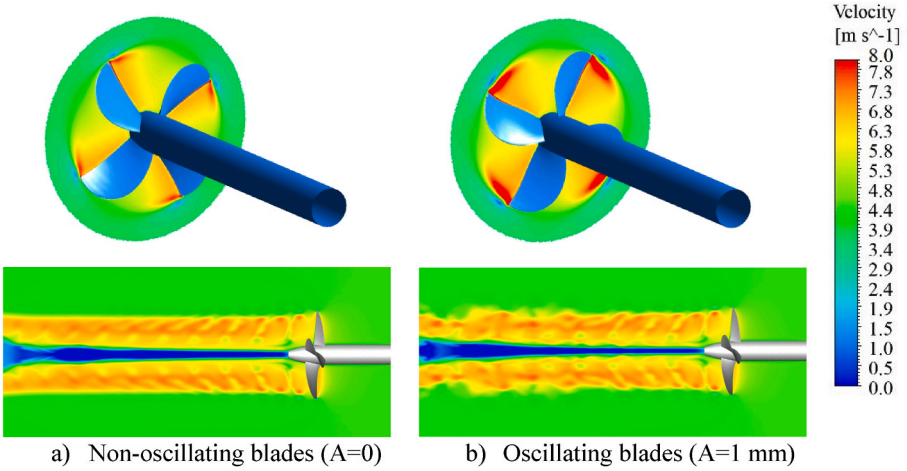

Fig. 9. Velocity fields around the oscillating and non-oscillating propeller blades captured on the rotor plane (above) and the meridional plane (below).

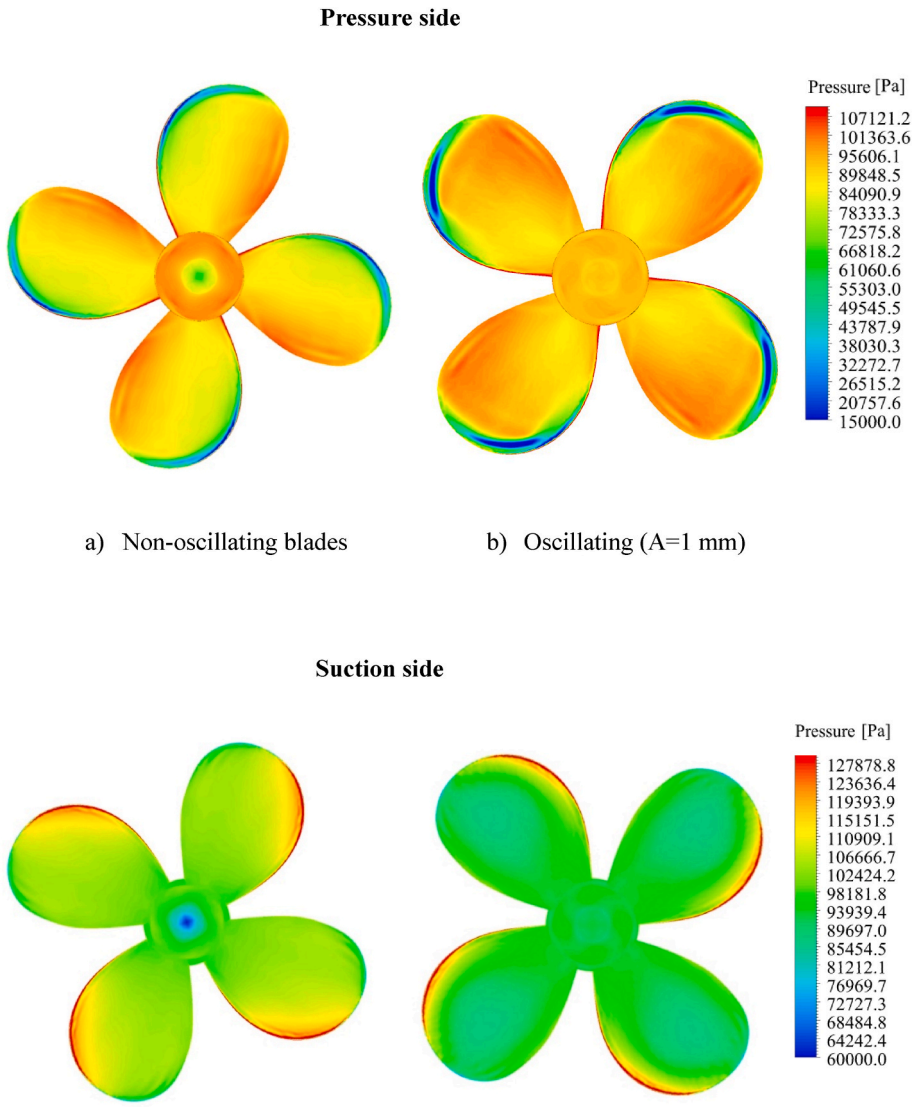

Fig. 10. Pressure contours on the pressure and suction surfaces of both oscillating and non-oscillating blades at vibration amplitude A = 1 mm.

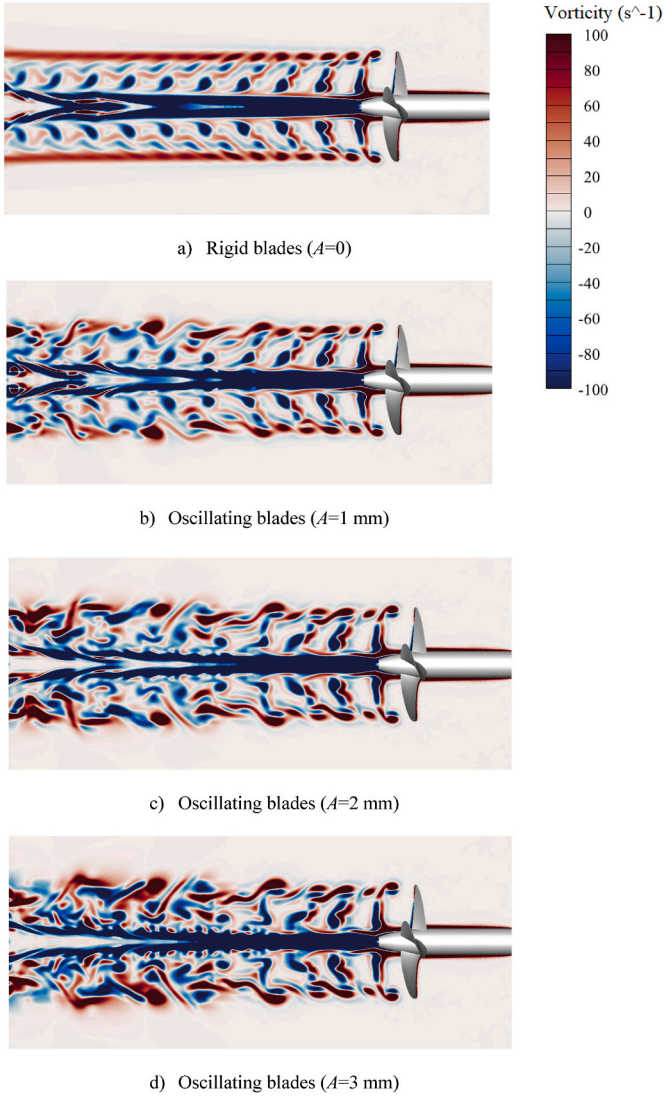

Fig. 11. Vortex shedding from the non-oscillating blades and oscillating blades at different vibration amplitudes (A = 1, 2, and 3 mm).

where Ω is the control volume, S is the control surface, U is the set of conservative variables, $\vec{F}$ and $\vec{G}$ are the advective and diffusive parts of the fluxes, respectively, and S_T is the source term.

The above equation is expressed in a semi-discrete form as follows:

$$\frac{\partial}{\partial t}(U) = R(U) \tag{2}$$

where R is the lumped residual and source term as described in (Win Naung et al., 2021e).

Due to blade vibration, the source of flow unsteadiness is affiliated with the oscillatory motion of the blade structure which is defined by the frequency and amplitude of the desired vibration mode. Therefore, the conservative variables U can be decomposed into the mean value and fluctuation terms, and it is expressed by the Fourier series for a specified frequency ω and the number of harmonics h as follow:

$$U = \overline{U} + \sum_{h=1}^{H}[U_A \sin(h\omega t) + U_B \cos(h\omega t)] \tag{3}$$

where, $\overline{U}$, U_A, and U_B are the coefficients of the Fourier series. The first term and the second term of the right-hand side of the equation represent the time-averaged and fluctuation of the conservative variables, respectively. Substituting Equation (3) into (2) yields a new set of the unsteady Navier-Stokes equations (Equation (4)). Equations (3) and (4) are used to analyse the unsteady parameters of the flow variables subject to the periodic oscillation of the propeller blades.

$$\omega \sum_{h=1}^{H}[hU_A \cos(h\omega t) - hU_B \sin(h\omega t)] = R \tag{4}$$

The spatial discretisation is performed using a second-order accurate Central scheme, and the temporal discretisation is conducted using a 4-stage Runge-Kutta scheme. For turbulence modelling, a high-fidelity LES method is employed to resolve the turbulent and transitional flow structures accurately. Employing the LES method, the large-scale turbulent structures are resolved directly, and the small-scale turbulent structures are captured using an appropriate subgrid-scale (SGS) model. The well-known Smagorinsky SGS model is one of the most widely used models for LES simulations, and this model is used in the present study. It should be noted that the employed computational grid is generated to ensure the grid is sufficient to resolve at least 80% of the turbulent kinetic energy.

The Smagorinsky constant with the inertial range of the turbulent spectrum is estimated as:

$$C_s = \frac{1}{\pi}\left(\frac{2}{3C_k}\right)^{3/4} = 0.18 \tag{5}$$

To capture all necessary flow structures, the size of the timestep Δt should be small enough for a fluid particle to move just a fraction of the spacing of the grid l with the fluid velocity u as given by:

$$\Delta t = C_{FL}\frac{l}{u} \tag{6}$$

In this equation, C_{FL} is the CFL or Courant number which is kept between 0.5 and 1.

A nonlinear harmonic method, also known as a nonlinear frequency-domain solution method, is typically applied to the modelling and analysis of turbomachinery as it provides an elegant way of modelling flow nonlinearity and harmonic disturbances at an efficient and affordable computational cost. This method only demands one or two orders of magnitude less computation time compared to the conventional time-domain solution methods. This method is also employed in this study to compute the unsteady flow parameters and hydrodynamic damping, and they will be compared to the time-domain LES method to verify the accuracy of the frequency-domain method. Using a nonlinear harmonic solution method, a new set of the unsteady Navier-Stokes equations are solved in the frequency-domain by dividing the unsteady period into $N = (2h + 1)$ time levels and iteratively solving the system of nonlinear equations coupling all N time levels. The authors' previous studies (Win Naung et al., 2021b, 2021d) suggest that a minimum of 3 harmonics are required to resolve the necessary flow structures in the downstream wake region, and therefore, 3 harmonics are used in this paper. The solution obtained from the frequency-domain method can be reconstructed in time to produce the solution in time history.

For the modelling of fluid-structure interaction, a modal coupling method is employed to define the blade oscillation in the CFD simulation as explained in (Win Naung et al., 2021c, 2021e). A modal analysis is first performed using a commercial structural code ANSYS Mechanical 2022R1 based on a Finite Element (FE) method to determine the shapes of the deformation of the propeller blades which are made of FRP composite materials.

The governing equation for the solid mechanics of the propeller blades is given by:

$$[M]\frac{\partial^2 \vec{d}}{\partial t^2} + [C]\frac{\partial \vec{d}}{\partial t} + [K]\vec{d} = \vec{f} \tag{7}$$

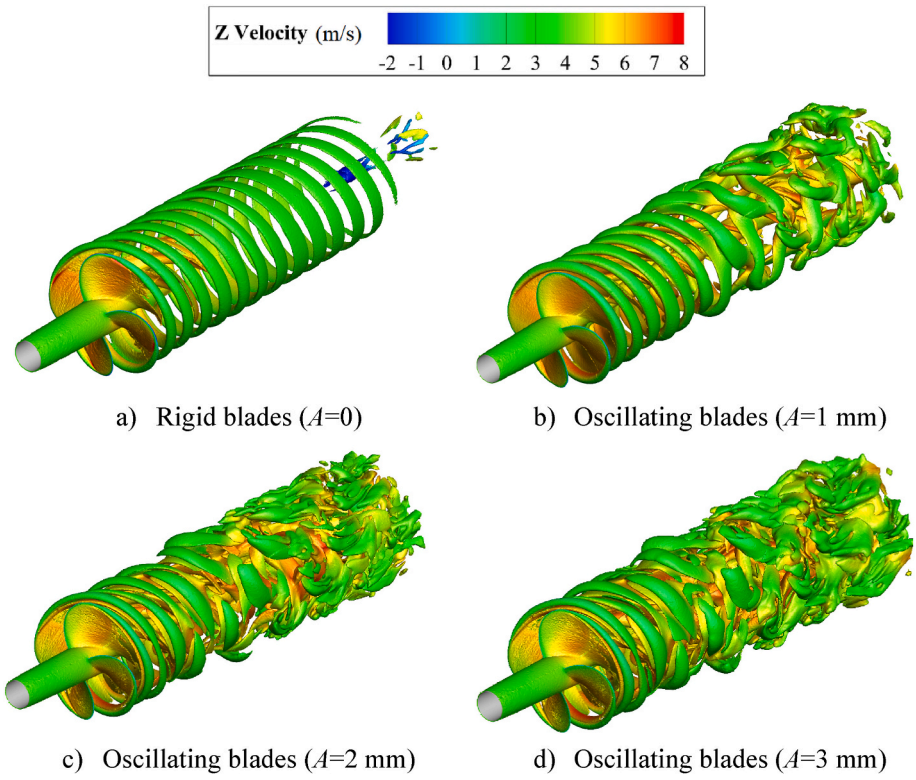

Fig. 12. Iso-surface of the vorticity generated from the rigid (non-oscillating) and flexible (oscillating) propeller blades.

where, $\vec{d}$ is the displacement, $\vec{f}$ is the external force applied to the propeller blades, and $[M]$, $[C]$, and $[K]$ are the mass matrix, the damping matrix, and the stiffness matrix, respectively.

The displacement of the propeller blades is expressed as:

$$\vec{d} = \sum_{i=1}^{n} q_i \vec{\varphi} \tag{8}$$

where, q_i and $\vec{\varphi}$ are the generalised displacement and the mode shapes of the propeller blades, respectively, and i is the number of modes.

The above equation can be expressed in matrix form as follow:

$$\vec{d} = [\varphi]\vec{q} \tag{9}$$

Equation (7) can be re-written by substituting Equation (9) and multiplying with $[\varphi]^T$ as:

$$[\varphi]^T[M][\varphi]\frac{\partial^2\vec{q}}{\partial t^2} + [\varphi]^T[C][\varphi]\frac{\partial\vec{q}}{\partial t} + [\varphi]^T[K][\varphi]\vec{q} = [\varphi]^T\vec{f} \tag{10}$$

Using the mass-normalised mode shapes and assuming a Rayleigh damping, the above equation becomes:

$$\frac{d^2q_i}{dt^2} + 2\xi_i\omega_i\frac{dq_i}{dt} + \omega_i^2 q_i = \vec{\varphi_i}^T\vec{f} \tag{11}$$

where, ω_i and ξ_i are the natural frequency and the damping coefficient of the system.

The natural frequencies and the mode shapes of the propeller blades are obtained from the modal analysis prior to the CFD simulations, and they are imported into the CFD simulations to facilitate the blade oscillation. The fundamental mode (first vibration mode) is considered to be the mode of vibration in this study. This study is designed to provide a detailed and in-depth analysis of the impact of the fundamental (first) vibration mode on the unsteady flow behaviours around a marine propeller. The fundamental vibration mode serves as the foundation for analysing more complex vibration phenomena. It provides insight into the basic behaviour of a structure when subjected to unsteady hydrodynamic loads. The first vibration mode of the propeller blade is illustrated in Fig. 4. To better visualise the blade deformation and oscillation, the undeformed shape of the blade is also added to the figure. The vibration frequency considered in this study is 60 Hz, and the amplitudes are varied from 1 mm (a relatively small amplitude) to 3 mm (a relatively large amplitude) in the simulations. The amplitude of the blade oscillation is specified using the generalised displacement as expressed by:

$$q_i(t) = \overline{q} + q_A \sin(\omega_i t) \tag{12}$$

where, $\overline{q}$ is the mean value and q_A is the amplitude of the oscillation of the propeller blade.

4. Results and discussion

The validation of the employed CFD model is initially carried out to ensure the CFD model is accurate and reliable. Fig. 5 presents the comparison of the performances of the propeller in terms of thrust coefficient (K_t), torque coefficient (K_q) and efficiency (η) obtained from the experiment and the simulations for different advanced ratios (J). The propeller's advanced ratio (J) can be defined as $J = U_0/n.D$, where U_0 is the advanced velocity and n is the rotational speed of the propeller. The torque and thrust coefficients and the propeller's efficiency (K_t, K_q, η) can also be expressed as (Wang et al., 2018):

$$K_{ti} = \frac{T_i}{\rho n^2 D^4} \tag{13}$$

$$K_{qi} = \frac{Q_i}{\rho n^2 D^5} \tag{14}$$

$$\eta = \frac{JK_{tx}}{2\pi K_{qx}} \tag{15}$$

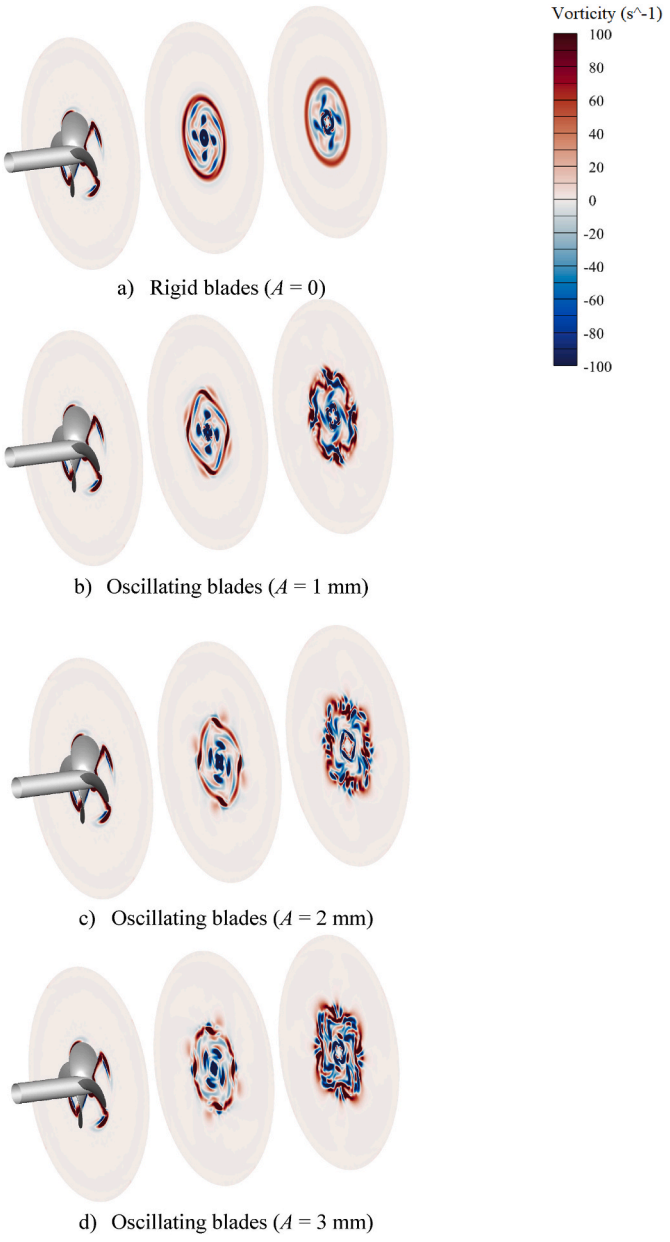

Fig. 13. Vorticity contours plotted on the planes normal to the flow direction at different locations in the downstream region.

where $i = x, y, z$ is the reference axis. T and Q are the thrust and torque forces, respectively. Despite some small deviations between the experiment and the simulations, it is, however, seen that the simulations predicted the turbine performances very well as a close agreement is obtained between the two methods. Both thrust coefficients and torque coefficients are decreasing with increasing advanced ratios. The maximum efficiency is found at approximately $K_t = 1.2$ and $K_q = 2$.

After having obtained a good agreement between the experiments and the simulations using a rigid (non-oscillating) blade, the accuracy of the CFD model is further tested for the oscillating propeller blades. As there are no experiments or previous numerical data for the case of oscillating blades, a direct comparison to the literature is not possible. Therefore, in this study, two different numerical methods such as the traditional time-domain LES method and the nonlinear frequency-domain LES method, which solves the flow governing equations in the frequency domain as discussed in Section 3, are employed, and the results are compared to each other. Upon finishing the simulation using the frequency-domain approach, it is necessary to reconstruct the flow solution in the time domain, as explained in the authors' previous study (Win Naung et al., 2021a). This reconstruction enables the extraction of unsteady flow data over time, which can then be employed for a comparative analysis with the time-domain method. The employed frequency-domain technique possesses the capability to accurately recreate the harmonic solution in time history. Fig. 6 compares the thrust coefficient and the torque coefficient over three oscillation cycles, obtained from the time-domain method and the frequency-domain method. It is observed that the results are close to each other, which instils greater confidence in the accuracy of the numerical model. Furthermore, to ensure that the flow structures resolved by the employed CFD model are reliable, the vorticity generated by the CFD model for the non-oscillating blade is compared to the image captured in an experiment conducted by (Felli et al., 2011). As seen in Fig. 7, the employed CFD model produces similar vorticity patterns as the experiment. Therefore, both quantitative and qualitative comparisons indicate that the CFD model employed in this study can be reliably used for further analysis.

The numerical investigations are further extended by integrating the blade vibration into the flow computation to analyse the effects of the flexible motion of the blades on the propeller performance and the unsteady flow behaviours. Firstly, the time-averaged pressure coefficient distributions over the surfaces of the blade are computed at the midsection of the blade from the cases using a rigid blade and an oscillating blade for two different advanced ratios ($J = 0.60$ and $J = 0.80$). These comparisons can be seen in Fig. 8. Although it is expected that the time-averaged pressure distribution of a periodically oscillating blade is similar to that of the non-oscillating blade, it is also found that the blade vibration has an impact on the pressure distribution on the blade surfaces. The propeller blade motion triggers a sudden change in the angle of attack throughout the vibration cycle, which leads to a transient behaviour in the flow interaction with the blade hydrofoil at the leading edge. As a result, a great difference in the pressure distribution, initiated from the leading edge and travelled towards the trailing edge, on both pressure and suction surfaces of the propeller blade between the rigid blade case and the vibrating blade case at $J = 0.80$ is observed.

Fig. 9 demonstrates the velocity contours extracted from the non-oscillating blade case and the oscillating blade case at the oscillation amplitude $A = 1$ mm. The velocity contours are plotted on the meridional plane (lower figures) and on the plane normal to the flow direction (upper figures). These figures show the difference in the velocity field between the two cases (oscillating and non-oscillating blade cases). It can be seen in the figures that the rotation of an oscillating blade leaves a higher velocity field, and the blade oscillation triggers a stronger tip vortex generation, which adds more disturbances to the downstream flow. Consequently, the downstream wake region is distorted and disorganised compared to the non-oscillating blade case. On the other hand, a recurring pattern of the velocity field is observed in the case of non-oscillating blades with the flow merging and losing its intensity in the far wake region.

The instantaneous pressure distributions over the pressure and suction surfaces of the propeller blades are presented in Fig. 10 for both non-oscillating and oscillating blade cases. The flow interaction with the blade hydrofoil at the leading edge of the blade and the generation of tip vorticity leads to a pressure difference between the pressure and suction surfaces of the propeller blade. The pressure is generally higher on the pressure surface and lower on the suction surface. A higher-pressure distribution over the pressure surface is more dominant in the case of an oscillating blade, whereas it is only detected nearly half of the pressure surface in the case of a non-oscillating blade. A pressure drop from the pressure surface to the suction surface is more pronounced when the blade is oscillating as a lower-pressure field is identified in the mid-region of the suction surface of the propeller blade. These figures indicate that the blade vibration has a significant effect on the pressure

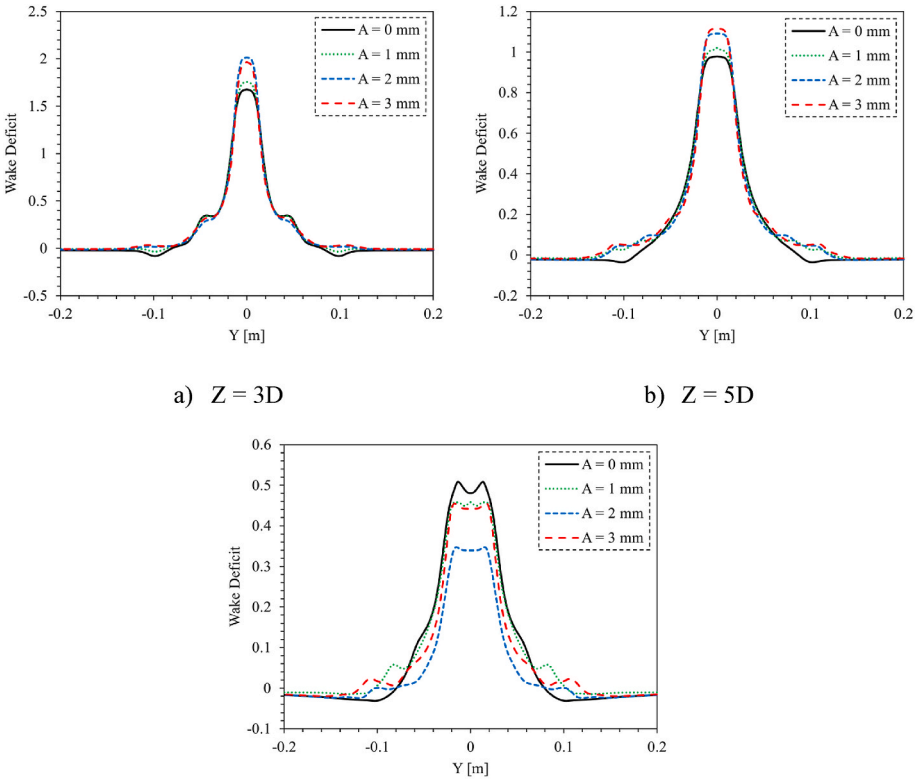

Fig. 14. Wake profiles in the downstream region of the propeller at Z = 3D, 5D, and 7D.

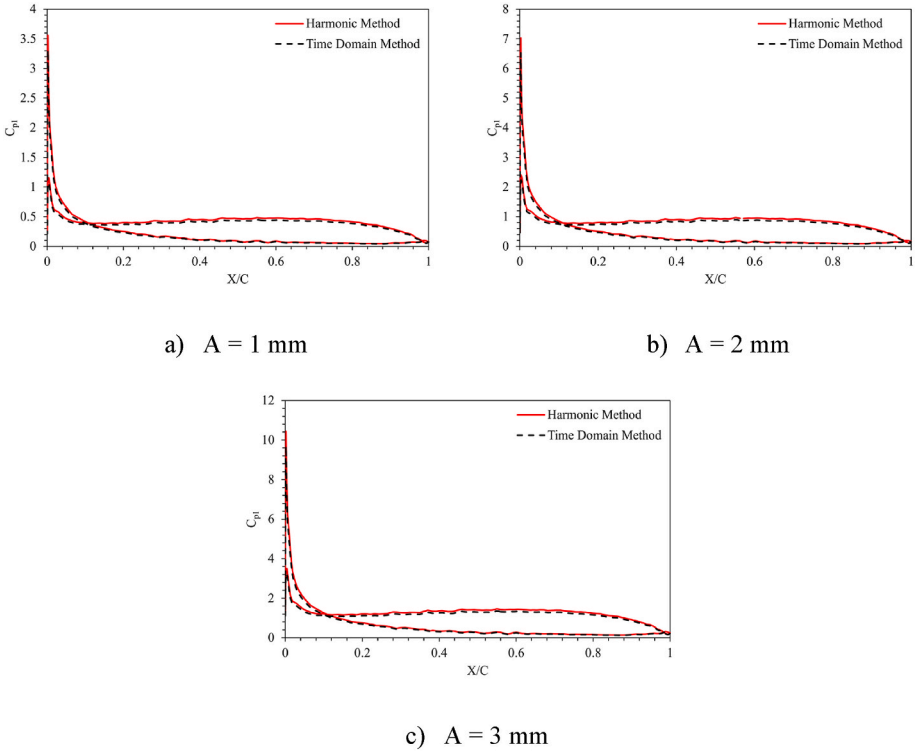

Fig. 15. Unsteady pressure amplitude coefficient (C_{pI}) distribution over the propeller, obtained from the time-domain and frequency-domain methods.

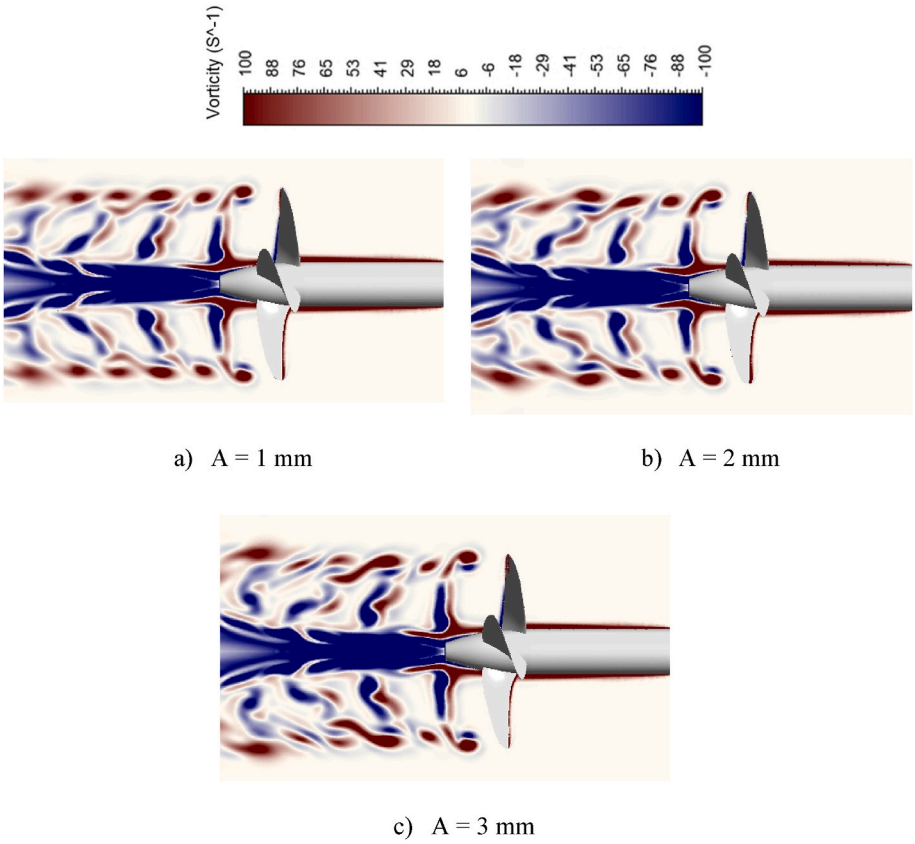

Fig. 16. Streamwise vorticity contours within the initial oscillation cycles obtained from the frequency-domain solution method.

distribution on the blade surfaces. This is because the angle of attack is continuously changing in time throughout the vibration cycle, which causes flow acceleration and deceleration on both surfaces of the blade, and in addition, the blade vibration triggers a stronger vortex generation that adds flow disturbances and unsteadiness to the blade surfaces. As a consequence, the pressure distribution over the blade surfaces is highly affected by the blade movement.

Fig. 11 presents the streamwise vorticity contours for the evolution of the tip vorticity and the development of the downstream vorticity from the non-oscillating and oscillating propellers at different vibration amplitudes (A = 1, 2 and 3 mm). A significant difference can be seen in the perturbation of the propeller on the unsteady flow field and downstream wake structures between the two cases. Vortex structures are more organised in the case of the non-oscillating propeller. The tip vorticity loses its intensity in the far wake area. The blade oscillation triggers a stronger vortex generation and induces more disturbances to the downstream flow, which causes earlier vortex merging and instability in the downstream wake. The periodic motion of the propeller blades results in a rapid acceleration in the vortex shedding and mixing. The vibration-induced instability becomes stronger at higher vibration amplitudes. At A = 1 mm, a chaotic pattern of the tip vortex and blade vortex is seen due to the oscillation of the propeller blades. These vortex structures interrupt and mix up with the recirculated hub vortices, which destabilises the behaviour of the downstream wake. Raising the vibration amplitude to 2 mm expedites the interaction and merging of the vortex structures among the hub, blade, and tip vortices. This behaviour becomes more intense at A = 3 mm, and some small-scale vortices are seen as a result of the vortex-to-vortex interaction. Overall, it is clear that the blade vibration has a significant influence on the evolution and development of the vorticity and the downstream wake structures. Furthermore, it is also noted that the resolution of the computational mesh is sufficiently fine enough to resolve both large and small-scale flow structures.

The instantaneous iso-surfaces of vorticity generated from the rigid (non-oscillating) and flexible (oscillating) propeller blades at different amplitudes are illustrated in Fig. 12. The vorticity structures are coloured by the axial velocity. In the case of the rigid blades, a continuous pattern of helical vortex structures, generated from the blade tips, is observed. The tip vorticity remains relatively stable to a certain extent before losing its strength, whereas the hub vorticity is completely distorted in the far downstream region. The oscillating blades, on the other hand, cause the deformation and breaking down of both the tip and hub vortices. The vortex generation process and distortion of the vortex structures are amplified by the oscillation of the propeller blades. The elliptic instability of the tip vorticity can be seen at all vibration amplitudes; however, the instability becomes stronger at higher amplitudes. The vortex mixing and breaking down happens quicker as the vibration amplitude is increased. Compared to the A = 1 mm case, the instability of the wake is considerably stronger at A = 3 mm as a result of an escalation of the vortex generation and early breaking down of the vortex structures due to a relatively higher amplitude of the blade oscillation.

In order to better visualises the mechanism of the evolution of the tip, blade and hub vorticity, the vorticity structures are plotted on the planes normal to the flow direction at Z = 0 (propeller rotor plane), 4.5D and 9D, where D is the propeller diameter, as shown in Fig. 13. It is observed that the initial development of tip vorticity at Z = 0 is similar in all cases. Early deformation of vortex structures due to the blade oscillation can be clearly seen in this figure. At Z = 4.5D, the distortion of the vorticity is more pronounced at the amplitudes of A = 2 mm and 3 mm. At Z = 9D, the vorticity is completely distorted in all cases of the blade oscillation with stronger structures at higher amplitudes as a consequence of the early breaking down of the vortex structures. In contrast to the non-oscillating blades, the oscillating propeller blades significantly influence the evolution of the downstream wake and unsteady flow behaviour. As the amplitude of the blade oscillation is raised, the instability of

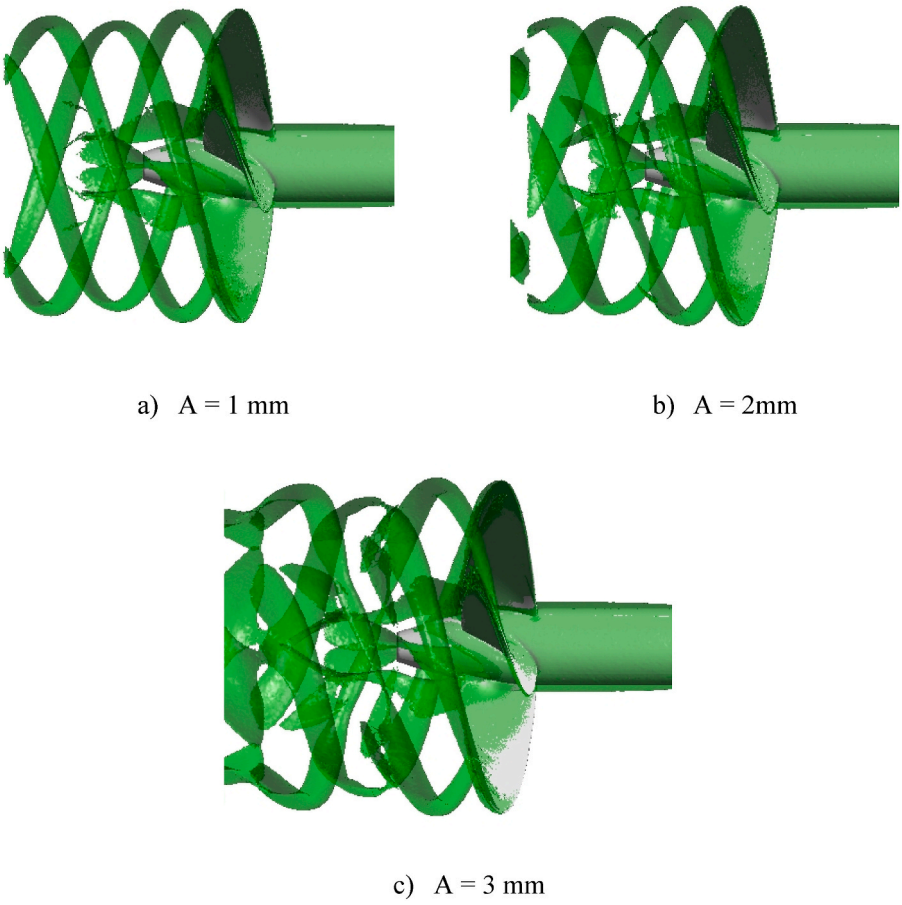

Fig. 17. Iso-surface of vorticity within the initial oscillation cycles obtained from the frequency-domain solution method.

Table 1
Hydrodynamic damping predicted by the time-domain solution method and the frequency-domain solution method.

Method	Hydrodynamic Damping
Time-domain Solution Method	0.185
Frequency-domain Solution Method	0.197

the downstream wake becomes higher with stronger vortex-to-vortex interactions among the tip, blade and hub vortices.

Fig. 14 demonstrates the wake profiles extracted along the vertical line in the Y-direction at different downstream locations for the cases of non-oscillating and oscillating propeller blades. Y = 0 marks the centre of the propeller hub, and positive and negative values represent the above and below of the centre point, respectively. It is seen that the peaks are found at the centre of the hub (Y = 0) where the velocity is low due to the hub vortex shedding. The peaks of the oscillating blades are higher than that of the non-oscillating blades in the cases of Z = 3D and Z = 5D. At Z = 3D, the highest peak of the wake profile is found at the amplitude of A = 2 mm where the pressure is low in the near wake region, whereas the peak is observed at A = 3 mm at Z = 5D. In contrast, the non-oscillating blade case sees the highest peak in the far wake region, at Z = 7D, whilst the oscillating blade at the amplitude of A = 2 mm possesses the lowest peak among all cases. The deflection of the shape of the wake profiles is observed at Z = 7D in both oscillating and non-oscillating blade cases due to the merging of the vortex structures in the far wake region; however, the deformation is more pronounced at the blade tip regions in the oscillating blade cases due to the stronger tip vorticity and mixing of the tip vortices. The magnitude of the wake profiles reduces as it goes further downstream.

As discussed in Section 3, a nonlinear harmonic solution method is also applied to this study to determine the capabilities of a frequency-domain method for the analysis of propellers. The oscillation of the propeller results in a variation of pressure over the surfaces of the blades, and the unsteady pressure variation can be split into the time-averaged value and amplitude of fluctuations based on the Fourier series. Fig. 15 compares the unsteady pressure amplitude coefficient, C_{p1}, obtained from the time-domain and frequency-domain methods. As seen, they are in close agreement, which indicates that the frequency-domain method can predict the unsteady variation over the blade surfaces, resulting from the oscillation of the propeller. It is also observed that the pattern of unsteady pressure variation over the propeller surface remains the same at different oscillation amplitudes; however, C_{p1} becomes higher as the amplitude of the oscillation is increased. This is mainly because the pressure fluctuations over the surfaces of the propeller become higher as the oscillation amplitude gets larger.

Fig. 16 presents the streamwise vorticity contours at different oscillation amplitudes for the initial periods of oscillation, exported from the frequency-domain solution. It is observed that the evolution of vorticity structures over the oscillating propellers is in good agreement with the vorticity predicted from the time-domain solution, illustrated in Fig. 11. This shows that the frequency-domain solution method can produce high-resolution flow structures, and the selected 3 harmonics are considered enough to resolve the necessary flow structures. To highlight the effects of the oscillation amplitude on the vortex generation process over the propellers, the iso-surface of vorticity within the initial oscillation periods at different oscillation amplitudes, obtained from the frequency-domain solution, are demonstrated in Fig. 17. The amplitude of oscillation has a pronounced effect on the vortex generation process, as clearly seen in the figure. Raising the amplitude adds

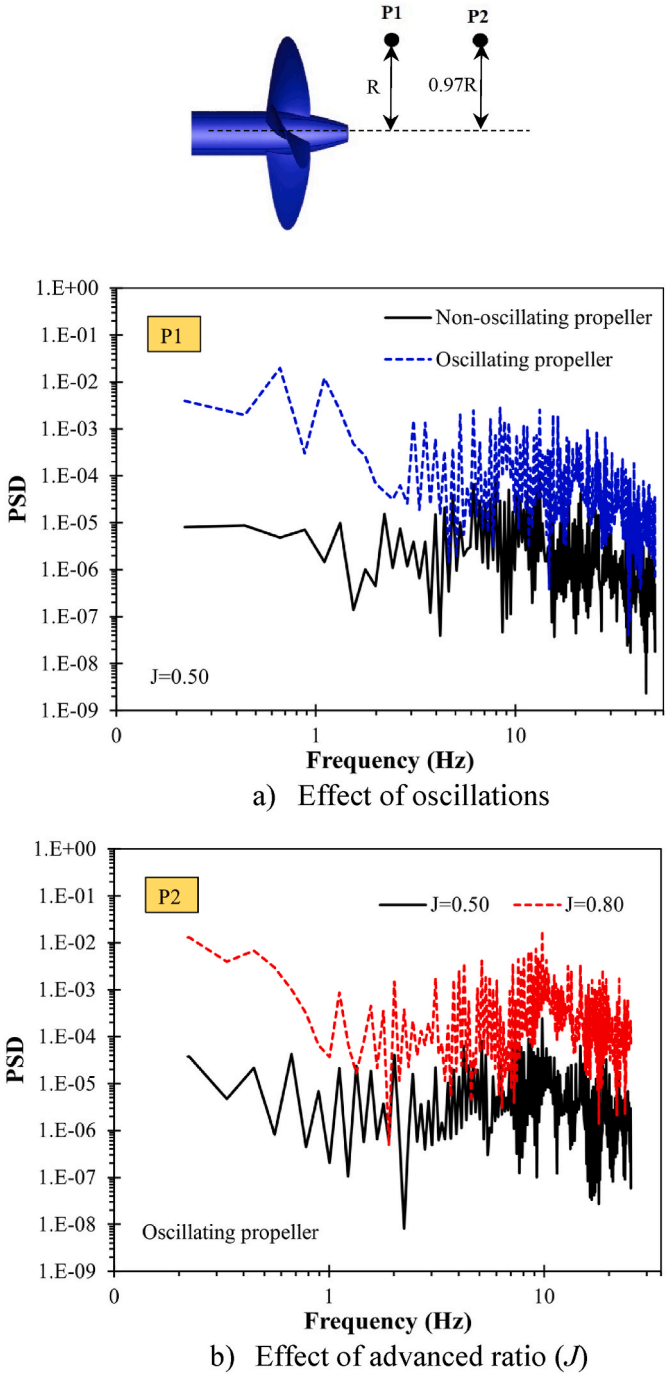

Fig. 18. The effects of oscillation and advanced ratio on power spectral density (PSD).

more disturbances to the evolution of tip vorticity, and the flow becomes turbulent due to the disruption, breaking down, and mixing of the vortex structures.

The hydrodynamic damping, computed as the hydrodynamic work per oscillation cycle, is used to determine the stability of the propellers. In this study, the value of hydrodynamic damping is predicted by both the time-domain and frequency-domain solution methods and the results are presented in Table 1. It is found that the hydrodynamic damping values predicted by both methods are in good agreement and the differences between the two methods are within an acceptable range. A positive hydrodynamic damping indicates that the blade oscillation is stable, whereas a negative value means that the propeller experiences a destabilising effect. A positive value is obtained in this analysis, which shows that the oscillation of the propeller is considered stable.

In terms of the computational cost, the harmonic solution method only requires 15 h while the conventional time-domain solution method demands two weeks on an HPC cluster using 100+ cores. The same computational resources are utilised for both methods. Therefore, it can be noted that the nonlinear frequency-domain solution method or the harmonic solution method can reliably predict the unsteady flow behaviour and parameters, and the hydrodynamic damping to determine the stability of the propellers, at a significantly reduced computational cost in comparison to the traditional time-domain LES method.

The power spectral density of pressure signals at two different points (P1 and P2) in the wake region of the oscillating propeller is shown in Fig. 18. The effects of oscillations at A = 2 mm compared to the rigid propeller blades are provided in Fig. 18 (a). It is observed that, at a specific distance (P1) in the downstream region of the blades, stronger perturbations are detected. The blade has caused greater vorticities in the closest probing point. The fluctuations in the oscillating case exceed those in the rigid blades since the interference between vortex generation causes more unstable propagation of the kinetic energy. It is also observed in Fig. 18 (b) that increasing the advanced ratio from $J = 0.5$ to 0.8 will also increase the kinetic energy in the wake region of the blade. This behaviour is mainly because the intervention among the adjacent tip vortices is powerful because of the short gaps between them.

5. Conclusions

In this numerical study, high-fidelity numerical simulations have been conducted over marine propeller blades, considering the flexibility of the blades. A modal analysis was performed to evaluate the natural frequencies and the mode shapes of the propeller blades which are made of FRP composite materials. The fundamental (first) vibration mode is mainly considered in this analysis as this is a crucial mode of vibration, and understanding the flow behaviour at the first natural frequency and first vibration mode can provide a great insight into more complex structural phenomena. The impact of the structural oscillations at a specific vibration frequency and amplitude on the physical characteristics of the propeller blades was investigated using a high-fidelity LES method. A frequency-domain solution method is also employed in addition to the typical time-domain solution method to investigate the capabilities of the frequency-domain method. The main findings of the present study can be summarised as follow.

- The flexibility of the blade has a noticeable impact on the pressure distribution on the propeller blade surfaces. The propeller blade motion triggers a sudden change in the angle of attack throughout the vibration cycle, which leads to a transient behaviour in the flow interaction with the blade hydrofoil at the leading edge.
- The flexibility of the oscillating propeller blade imposes additional flow disturbance and stronger tip vortex generation, which adds more perturbations to the downstream flow. Consequently, the downstream wake region is distorted and disorganised compared to the rigid blade case.
- The periodic motion of the propeller blade results in a rapid acceleration in the vortex shedding and mixing. The vibration-induced instability gets stronger at large vibration amplitudes.
- The unsteady pressure amplitude coefficient distribution over the surfaces of the propeller blades becomes higher at greater oscillation amplitudes due to stronger flow perturbations.
- A frequency-domain solution method accurately predicted the unsteady pressure distribution, vortex generation, and hydrodynamic damping in contrast to the time-domain solution. The frequency-domain method, however, only demands one to two orders of magnitude less computational cost.

Overall, the blade oscillation can impose significant implications in the pressure distribution, vortex generation, and cavitation process, which has a direct impact on the structural integrity of the marine propellers, and this needs to be taken into account during the design process. It is also understood that understanding higher vibration modes is important for predicting how higher modes interact with each other and with external forces, and the present study will be extended by exploring higher vibration modes in the future studies.

CRediT authorship contribution statement

Shine Win Naung: Conceptualization, Methodology, Software, Validation, Formal analysis, Investigation, Writing – original draft, Visualization. **Mahdi Erfanian Nakhchi:** Formal analysis, Writing – review & editing. **Mohammad Rahmati:** Conceptualization, Methodology, Writing – review & editing, Supervision.

Declaration of competing interest

The authors declare that they have no known competing financial interests or personal relationships that could have appeared to influence the work reported in this paper.

Data availability

Data will be made available on request.

References

Borg, M.G., Xiao, Q., Allsop, S., Incecik, A., Peyrard, C., 2021. A numerical structural analysis of ducted, high-solidity, fibre-composite tidal turbine rotor configurations in real flow conditions. Ocean Eng. 233, 109087.

Chen, F., Liu, L., Lan, X., Li, Q., Leng, J., Liu, Y., 2017. The study on the morphing composite propeller for marine vehicle. Part I: design and numerical analysis. Compos. Struct. 168, 746–757.

Dubbioso, G., Muscari, R., Di Mascio, A., 2013. Analysis of the performances of a marine propeller operating in oblique flow. Comput. Fluid 75, 86–102.

Felli, M., Camussi, R., Di Felice, F., 2011. Mechanisms of evolution of the propeller wake in the transition and far fields. J. Fluid Mech. 682, 5–53.

Felli, M., Di Felice, F., Guj, G., Camussi, R., 2006. Analysis of the propeller wake evolution by pressure and velocity phase measurements. Exp. Fluid 41, 441–451.

Felli, M., Roberto, C., Guj, G., 2009. Experimental analysis of the flow field around a propeller–rudder configuration. Exp. Fluid 46, 147–164.

Gonabadi, H., Oila, A., Yadav, A., Bull, S., 2022. Fatigue life prediction of composite tidal turbine blades. Ocean Eng. 260, 111903.

Gong, J., Guo, C.-Y., Zhao, D.-G., Wu, T.-C., Song, K.-W., 2018. A comparative Des study of wake vortex evolution for ducted and non-ducted propellers. Ocean Eng. 160, 78–93.

Kumar, P., Mahesh, K., 2017. Large eddy simulation of propeller wake instabilities. J. Fluid Mech. 814, 361–396.

Long, Y., Long, X., Ji, B., Huang, H., 2019. Numerical simulations of cavitating turbulent flow around a marine propeller behind the hull with analyses of the vorticity distribution and particle tracks. Ocean Eng. 189, 106310.

Muscari, R., Dubbioso, G., Di Mascio, A., 2017. Analysis of the flow field around a rudder in the wake of a simplified marine propeller. J. Fluid Mech. 814, 547–569.

Naung, S.W., Nakhchi, M.E., Rahmati, M., 2021a. An experimental and numerical study on the Aerodynamic performance of vibrating wind turbine blade with Frequency-domain method. J Appl Computat Mechan 7, 1737–1750.

Naung, S.W., Nakhchi, M.E., Rahmati, M., 2021b. Prediction of flutter effects on transient flow structure and aeroelasticity of low-pressure turbine cascade using direct numerical simulations. Aero. Sci. Technol. 119, 107151.

Pemberton, R., Summerscales, J., Graham-Jones, J., 2018. Marine Composites: Design and Performance. Woodhead Publishing.

Pereira, F., Salvatore, F., Di Felice, F., Soave, M., 2004. Experimental investigation of a cavitating propeller in non-uniform inflow. In: Proceedings of the 25th Symposium on Naval Hydrodynamics. Canada, St. John's.

Phillips, A.W., Cairns, R., Davis, C., Norman, P., Brandner, P.A., Pearce, B.W., Young, Y., 2017. Effect of material design parameters on the forced vibration response of composite hydrofoils in air and in water. Fifth Int Sympos Marine Propulsors 813–822.

Politis, G.K., 2004. Simulation of unsteady motion of a propeller in a fluid including free wake modeling. Eng. Anal. Bound. Elem. 28, 633–653.

Posa, A., Broglia, R., Balaras, E., 2020. Flow over a hydrofoil in the wake of a propeller. Comput. Fluid 213, 104714.

Rahmati, M.T., 2009. Application of A pressure correction method for modeling incompressible flow through turbomachines. Int. J. Comput. Methods 6, 399–411.

Rama Krishna, V., Sanaka, S.P., Pardhasaradhi, N., Raghava Rao, B., 2022. Hydro-elastic computational analysis of a marine propeller using two-way fluid structure interaction. J. Ocean Eng. Sci. 7, 280–291.

Vardhan, D.H., Ramesh, A., Reddy, B.C.M., 2019. A review on materials used for marine propellers. Mater. Today: Proc. 18, 4482–4490.

Wang, L., Guo, C., Su, Y., Xu, P., Wu, T., 2017. Numerical analysis of a propeller during heave motion in cavitating flow. Appl. Ocean Res. 66, 131–145.

Wang, L., Guo, C., Xu, P., Su, Y., 2018. Analysis of the performance of an oscillating propeller in cavitating flow. Ocean Eng. 164, 23–39.

Wang, L., Martin, J.E., Felli, M., Carrica, P.M., 2020. Experiments and Cfd for the propeller wake of a generic submarine operating near the surface. Ocean Eng. 206, 107304.

Wildy, S., Cazzolato, B., Kotousov, A.G., 2010. Detection of Delamination Damage in a Composite Laminate Beam Utilising the Principle of Strain Compatibility. Key Engineering Materials. Trans Tech Publ, pp. 269–272.

Win Naung, S., Nakhchi, M.E., Rahmati, M., 2021a. High-fidelity Cfd simulations of two wind turbines in arrays using nonlinear frequency domain solution method. Renew. Energy 174, 984–1005.

Win Naung, S., Nakhchi, M.E., Rahmati, M., 2021b. Prediction of flutter effects on transient flow structure and aeroelasticity of low-pressure turbine cascade using direct numerical simulations. Aero. Sci. Technol. 119, 107151.

Win Naung, S., Rahmati, M., Farokhi, H., 2021c. Aeromechanical analysis of a complete wind turbine using nonlinear frequency domain solution method. J. Eng. Gas Turbines Power 143, 011018.

Win Naung, S., Rahmati, M., Farokhi, H., 2021d. Direct numerical simulation of interaction between transient flow and blade structure in a modern low-pressure turbine. Int. J. Mech. Sci. 192, 106104.

Win Naung, S., Rahmati, M., Farokhi, H., 2021e. Nonlinear frequency domain solution method for aerodynamic and aeromechanical analysis of wind turbines. Renew. Energy 167, 66–81.

Yilmaz, N., Dong, X., Aktas, B., Yang, C., Atlar, M., Fitzsimmons, P.A., 2020. Experimental and numerical investigations of tip vortex cavitation for the propeller of a research vessel, "The Princess Royal". Ocean Eng. 215, 107881.

Young, Y.L., Motley, M.R., Barber, R., Chae, E.J., Garg, N., 2016. Adaptive Composite Marine Propulsors and Turbines: Progress and Challenges, vol. 68. Applied Mechanics Reviews.